Mobility of solitons in one-dimensional lattices with the cubic-quintic nonlinearity

C. Mejía-Cortés* and Rodrigo A. Vicencio
Departamento de Física and MSI-Nucleus on Advanced Optics, Center for Optics and Photonics (CEFOP), Facultad de Ciencias, Universidad de Chile, Santiago, Chile

Boris A. Malomed
Department of Physical Electronics, School of Electrical Engineering, Faculty of Engineering, Tel Aviv University, Tel Aviv 69978, Israel
(Received 17 September 2013; published 5 November 2013)

We investigate mobility regimes for localized modes in the discrete nonlinear Schrödinger (DNLS) equation with the cubic-quintic on-site terms. Using the variational approximation, the largest soliton's total power admitting progressive motion of kicked discrete solitons is predicted by comparing the effective kinetic energy with the respective Peierls-Nabarro (PN) potential barrier. The prediction, for the DNLS model with the cubic-only nonlinearity too, demonstrates a reasonable agreement with numerical findings. A small self-focusing quintic term quickly suppresses the mobility. In the case of the competition between the cubic self-focusing and quintic self-defocusing terms, we identify parameter regions where odd and even fundamental modes exchange their stability, involving intermediate asymmetric modes. In this case, stable solitons can be set in motion by kicking, so as to let them pass the PN barrier. Unstable solitons spontaneously start oscillatory or progressive motion, if they are located, respectively, below or above a mobility threshold. Collisions between moving discrete solitons, at the competing nonlinearities frame, are studied too.

DOI: 10.1103/PhysRevE.88.052901 PACS number(s): 05.45.−a, 42.25.Dd, 42.65.Tg, 72.15.Rn

I. INTRODUCTION

Diffraction of light and matter waves upon propagation is a commonly known fundamental effect. A wave tends to spread over the whole space as it evolves. However, when the medium is sensitive to the intensity of traveling waves, nonlinear corrections must be included in the description of the wave propagation, which often leads to adequate models based on nonlinear partial differential equations (PDEs). Solitary-wave solutions, or *solitons*, are robust localized modes generated by this type of nonlinear evolution equations. Arguably, one of the most generic PDEs related to these systems is the nonlinear Schrödinger (NLS) equation. In the context of optics, it predicts the existence of effectively one-dimensional (1D) solitons in optical fibers [1] and planar wave guides [2].

Still richer phenomenology emerges when the nonlinear media include a periodic transverse modulation of local properties. Nonlinearity and periodicity combine to offer a wide range of phenomena which have no counterparts in bulk homogeneous media. Among them, a great deal of interest has been drawn to discrete solitons [3–6]. Numerous realizations of discrete solitons have been established, ranging from nonlinear optics (guided waves in inhomogeneous optical structures [7] and photonic-crystal lattices [8,9]) to atomic physics (chains of droplets of Bose-Einstein condensates (BECs) trapped in deep spatially periodic potentials, [10–12], including dipolar BECs with the long-range interaction between the drops [13,14]) and from solid-state settings (Josephson-junction ladders [15–17]) to biophysics, in various models of the DNA double strand [18,19].

Robust mobility of fundamental modes is a necessary ingredient underlying the transport of light or matter through the lattice. A vast set of theoretical predictions [20–22] and experimental observations [23,24] addressed the issue of the mobility of discrete solitons in photonic lattices with the cubic (Kerr) nonlinearity, as well as with saturable [25] and quadratic (second-harmonic-generating) [26] nonlinear responses. Recently, it was also analyzed in the model of the photonic lattice with a saturable nonlinearity [27] and in an array of coupled optical resonators [28]. Adopting the cubic-quintic (CQ) form of the on-site nonlinear terms, i.e., including the second-order Kerr corrections to the refractive index, the solitons have been observed traveling across the lattice after being precisely kicked [29]. As concerns applications, a system that exhibits good mobility of localized modes may be promising for the design of all-optical networks, where mobility can help to implement fast switching and transfer of signals across the system.

In this work we focus on the existence and stability of mobile fundamental localized modes, both odd and even ones (alias on-site and off-site-centered states, respectively), in the discrete NLS (DNLS) equation with CQ on-site nonlinearities. First we develop an analytical approach predicting, with the help of the variational approximation (VA), the *mobility threshold* in this model, i.e., the largest value of the total power (alias norm) of the discrete soliton admitting its progressive motion induced by the initial kick. The threshold is predicted by equating the largest possible value of effective kinetic energy of the kicked soliton to the height of the corresponding Peierls-Nabarro (PN) barrier. The comparison of this analytical result for the usual DNLS lattice with the purely cubic nonlinearity with numerical results demonstrates a reasonable agreement. The VA-based prediction describes qualitatively correctly too fast suppression of the mobility of the discrete solitons with the increase of the self-focusing quintic nonlinear term. In the case of the competing combination of the self-focusing cubic and defocusing quintic terms, we emphasize the crucial role played by regions of the stability exchange between the odd

*Corresponding author: ccmejia@googlemail.com

and even fundamental modes and by intermediate asymmetric modes existing in those regions for the understanding of the *spontaneous mobility* featured by solitons which are unstable in the static state. We also study the mobility of stable discrete solitons under the action of the kick.

The rest of the paper is organized as follows. The model is formulated in Sec. II. The VA for the discrete solitons and the PN barrier are considered in the analytical form in Sec. III, the main result of which is the prediction of the above-mentioned mobility threshold. Numerical results for the system with the absolute-focusing nonlinearity are reported in Sec. IV (in particular, the analytically predicted mobility threshold is compared to numerical findings). The model with the competing focusing-defocusing CQ terms is considered, in the numerical form, in Sec. V. In this section, points of the stability exchange between the odd and even fundamental localized modes are analyzed at first, due to the specific role which, as said above, they play in the transition of unstable solitons into the state of spontaneous motion. The dynamical regimes proper, of both the spontaneous motion for originally unstable discrete modes and the motion of kicked stable solitons, are presented in that section too, along with basic results for collisions between moving discrete solitons. The paper is concluded by Sec. VI.

II. THE MODEL

We address the propagation of waves in nonlinear discrete systems which were studied in diverse physical contexts in the course of the last two decades [6,30–32]. In those systems, the discreteness appears as an effect of weak interaction between separated elements, basic examples being arrays of coupled optical wave guides or BECs trapped in deep optical lattices. In the context of optics, an evanescent coupling (linear interaction) between modes of adjacent wave guiding cores takes place when the wave guides are set in close proximity to each other. Considering this interaction in the lattice, a set of linearly coupled equations is derived, similar to the tight-binding models in solid-state physics [33]. Assuming a local (on-site) CQ nonlinear response of the system, we arrive at the 1D DNLS equation in the known form:

$$i\dot{\psi}_n + (\psi_{n+1} + \psi_{n-1}) + \gamma|\psi_n|^2\psi_n + \nu|\psi_n|^4\psi_n = 0. \quad (1)$$

Here $\psi_n(z)$ is the field amplitude at the nth lattice site, and $\dot{\psi}_n$ stands for its derivative with respect to the evolutional variable, which corresponds to the normalized propagation coordinate z in the present case (this model also applies to BECs loaded into a deep optical lattice, where the dynamical variable is time t). The intersite coupling constant is fixed here to be 1, but the coefficient in front of the on-site quintic term is a free parameter, ν. For $\gamma > 0$ and $\nu < 0$ (the competing on-site self-focusing cubic and self-defocusing quintic terms), static unstaggered solitons in this model were studied in detail in Ref. [34] and their 2D counterparts in Ref. [35].

Equations (1) conserve two dynamical invariants, namely, the total power, alias norm,

$$P = \sum_{n=-N}^{N} |\psi_n|^2, \quad (2)$$

and the Hamiltonian

$$H = -\sum_{n=-N}^{N}\left(\psi_{n+1}\psi_n^* + \psi_{n+1}^*\psi_n + \frac{\gamma}{2}|\psi|^4 + \frac{\nu}{3}|\psi|^6\right), \quad (3)$$

for a lattice of $2N+1$ sites.

First, we look for stationary solutions of Eqs. (1) of the usual form, $\psi_n(z) = \phi_n \exp(i\lambda z)$, where λ is to the longitudinal propagation constant, while ϕ_n defines a real spatial profile of the soliton. Linear solutions, in the case of $\gamma, \nu = 0$, correspond to plane waves $\phi_n = A\exp(ikn)$ that form the linear band of the system defined as $\lambda = 2\cos k$, where k is the transverse propagation constant. Thus, the linear band covers the region $\lambda \in (-2,2)$.

In the nonlinear system, with $\gamma, \nu \neq 0$, exponentially localized solutions for discrete solitons exist outside of the linear band, and they can be obtained by solving the following set of real coupled algebraic equations:

$$\lambda\phi_n = \phi_{n+1} + \phi_{n-1} + \gamma\phi_n^3 + \nu\phi_n^5. \quad (4)$$

By means of the high-confinement approximation [36], we construct an initial condition which is very close to an exact localized solution. Then, we implement an iterative multi-dimensional Newton-Raphson method to find a numerical solution for a given frequency λ or power P (both parameters can be used independently to find solutions). Once a solution is obtained, we vary the parameters to construct a whole family of discrete solitons. Then, we perform the standard linear stability analysis [37], obtaining an instability growth rate, g, for each solution. In our notation, $g = 0$ represents a stable solution, while $g > 0$ represents an unstable one. Hereafter, stable and unstable solutions are plotted by means of solid and dashed lines, respectively.

In the framework of this work, we focus on typical fundamental modes that are relevant to understand the dynamical properties of collective excitations in this type of lattices. Accordingly, we call an *odd mode* the one centered at one site of the lattice, while the *even mode* is centered between two lattice sites. Other frequently used names for these two species of the localized states are, respectively, on-site-centered and off-site-centered modes. The quantity which unequivocally identifies the species is the center-of-mass coordinate, defined as

$$X_{\rm cm} \equiv \frac{1}{P}\sum_{n=-N}^{N} n|\phi_n|^2. \quad (5)$$

Odd and even modes are singled out, severally, by integer and semi-integer values of $X_{\rm cm}$, respectively.

III. THE ENERGY BARRIER AND VARIATIONAL APPROXIMATION

A. The Peierls-Nabarro barrier

In DNLS models, the PN potential is a major concept for studying the mobility of localized modes. Odd and even states correspond to fundamental quiescent solutions. The difference in their Hamiltonian values defines the height of the PN potential barrier [38]. Indeed, for a given power (norm), this difference determines effective energetic barriers for moving

the discrete soliton across the lattice: To move the odd mode a single site across the lattice, it needs to be transformed into even mode and, again, to the odd mode centered at the next site. Thus, the energy required for this transformation must be at least equal to the energy difference between the two states, keeping the power constant (in the case of the adiabatic movement).

It is worthy to mention that different nonlinear interactions generate diverse energy landscapes. For example, a photorefractive saturable DNLS model [27,39,40] allows the existence of a single stability region for any fundamental solution and regions of multistability where intermediate asymmetric solutions appear. The continuous exchange of stability properties is accompanied by several crossings of the Hamiltonian values, generating diverse regions where the mobility is enhanced, even for high powers. Another interesting model is a dipolar DNLS one, applied for the description of BEC's with long-range interactions [41]. This cubic model possesses a single region of simultaneously unstable solutions, where the stable solution becomes the intermediate one. Good mobility occurs in the exchange regions, where Hamiltonian values approach and cross each other.

In this connection, it is also relevant to mention a very recent result for 2D cubic Kagome lattices [42]. For that model, it was found that a single stability-exchange region appears, where the intermediate solution becomes the ground state of the system. As the appearance of these solutions implies that the energy barriers decrease, coherent transport for very low power and highly localized modes were also found, which is an unusual property of 2D cubic lattices [6,30–32].

B. Variational approximation

The VA provides a first estimate about regions in the parameter space, where mobility may be expected. The VA was developed in Refs. [29,34,43] for 1D discrete solitons in the CQ-DNLS model, but considering only the self-defocusing sign of the quintic term. To apply the VA, the following *ansatz* was adopted:

$$\phi_n^{(\mathrm{VA})} = Ae^{-\alpha|n-n_0|}, \tag{6}$$

where amplitude A and inverse width α are real positive constants, and $n_0 = (\chi+1)/2$ defines the position of the center of the mode, with $\chi = 0$ and $\chi = 1$ for even and odd states, respectively. We here treat A as a variational parameter, while α is fixed by the substitution of ansatz (6) into the linearization of Eq. (4), for the decaying tail of the discrete soliton far from its center: $\lambda = 2\cosh\alpha$.

The power associated with ansatz (6) is

$$P = A^2\frac{\cosh(\chi\alpha)}{\sinh\alpha}. \tag{7}$$

It is well known that the Hamiltonian can be expressed as the Legendre transform of its Lagrangian, namely,

$$H(q_n,p_n) = \sum_{n=-\infty}^{+\infty}\dot{q}_n p_n - L(q_n,\dot{q}_n), \tag{8}$$

where, for model (1), canonical coordinates p_n and q_n correspond to ψ_n and $i\psi_n^*$, respectively. Thus, Eq. (4) corresponds to the following Lagrangian,

$$-L = \lambda P + H. \tag{9}$$

The substitution of ansatz (6) into Eq. (3) and the elimination of A^2 by means of Eq. (7) yields the effective Hamiltonians for the odd and even modes,

$$H_{\mathrm{odd}}^{\mathrm{VA}}(P) = -2\,\mathrm{sech}\,(\alpha)P - \frac{\gamma}{4}[\cosh(2\alpha)\,\mathrm{sech}^2(\alpha)\tanh(\alpha)] \times P^2 - \frac{\nu}{3}\left[\frac{2\cosh(2\alpha)-1}{2\cosh(2\alpha)+1}\tanh^2(\alpha)\right]P^3, \tag{10}$$

$$H_{\mathrm{even}}^{\mathrm{VA}}(P) = -2e^{-\alpha}\left[1+\sinh(\alpha)\right]P - \frac{\gamma}{4}\tanh(\alpha)P^2 - \frac{\nu}{3}\left[\frac{\sinh^2(\alpha)}{2\cosh(2\alpha)+1}\right]P^3. \tag{11}$$

Finally, by inserting the previous expressions for the Hamiltonian into Eq. (9), we obtain the full Lagrangian of the system for both fundamental modes as function of their width and power content:

$$L_{\mathrm{odd}}^{\mathrm{VA}}(P) = -2\sinh(\alpha)\tanh(\alpha)P + \frac{\gamma}{4}[\cosh(2\alpha)\,\mathrm{sech}^2(\alpha)\tanh(\alpha)]P^2 + \frac{\nu}{3}\left[\frac{2\cosh(2\alpha)-1}{2\cosh(2\alpha)+1}\tanh^2(\alpha)\right]P^3, \tag{12}$$

$$L_{\mathrm{even}}^{\mathrm{VA}}(P) = [1-\cosh(2\alpha)-2\sinh(\alpha)+\sinh(2\alpha)]P + \frac{\gamma}{4}\tanh(\alpha)P^2 + \frac{\nu}{3}\left[\frac{\sinh^2(\alpha)}{1+2\cosh(2\alpha)}\right]P^3. \tag{13}$$

The Euler-Lagrange equations obtained by these Lagrangians are

$$\frac{\partial}{\partial P}\left[L_{\mathrm{odd,even}}^{(\mathrm{VA})}\right] = 0. \tag{14}$$

To understand how the quintic term in Eq. (1) affects the mobility of localized solutions, it may be treated as a perturbation because, as shown below, quite small positive values of ν lead to full suppression of the mobility. Then, in the zero-order approximation ($\nu = 0$), Eqs. (14) and (12), for the odd modes and $\gamma = 1$, yield

$$P_{\mathrm{odd}}^{(0)}(\alpha) = 4(\cosh^2\alpha)(\sinh\alpha)\,\mathrm{sech}(2\alpha). \tag{15}$$

Next, we introduce the first-order correction to Eq. (15),

$$P_{\mathrm{odd}}(\alpha) = P_{\mathrm{odd}}^{(0)}(\alpha) + \nu P_{\mathrm{odd}}^{(1)}(\alpha), \tag{16}$$

for which the calculation based on the VA results yields

$$P_{\mathrm{odd}}^{(1)}(\alpha) = 32\frac{[2-\mathrm{sech}(2\alpha)](\cosh^5\alpha)\sinh^3\alpha}{[2\cosh(2\alpha)+1]\cosh^2(2\alpha)}. \tag{17}$$

To estimate the mobility threshold, it is necessary to find the *largest* values of α and P for which the kicked mode may be set in motion [6,44–48]. A kicked odd profile is obtained by adding the phase term to ansatz (6),

$$\phi_n^{(0)}\cdot e^{ikn} = Ae^{-\alpha|n|+ikn}, \tag{18}$$

where k is the real magnitude of the kick, which corresponds to a transverse propagation constant restricted to the interval of $[0,\pi]$. This kicked profile increases the effective Hamiltonian

of the odd mode by adding what, in the present context, plays the role of the *kinetic energy*:

$$E_{\rm kin} = 2\,\mathrm{sech}\,\alpha\,(1-\cos k)\,P. \tag{19}$$

Then, taking into regard that the Hamiltonian of the even mode is larger than for the odd one, the mobility limit is determined by equating Hamiltonian (10), modified according to ansatz (18) with $k=\pi$ [which implies taking the largest possible value of kinetic energy (19)], to the energy of the immobile even soliton, for the same total power P:

$$H_{\rm odd}^{\rm (VA)}(P,k=\pi) = H_{\rm even}^{\rm (VA)}(P). \tag{20}$$

This equations determines the largest values of the total power, $P_{\rm max}$, at which the kicked discrete soliton may be set in persistent motion.

First, in the cubic-only model ($\nu=0$), Eq. (20), with $H_{\rm odd,even}^{\rm (VA)}$ and P substituted by the VA results [see Eqs. (10), (11), and (15)], leads to the following equation for $\alpha_{\rm max}$, which corresponds to the respective mobility threshold $P_{\rm max}^{(0)}$:

$$\begin{aligned} &2\,(2+\sinh\alpha_{\rm max}+\tanh\alpha_{\rm max})\,(\cosh\alpha_{\rm max})\cosh(2\alpha_{\rm max}) \\ &\quad = \exp(\alpha_{\rm max})\sinh^4\alpha_{\rm max}, \end{aligned} \tag{21}$$

a numerical solution of which yields

$$\alpha_{\rm max} \approx 2.0361. \tag{22}$$

Finally, the substitution of this $\alpha_{\rm max}$ into the VA-predicted expression for the total power [see Eq. (15)] gives

$$P_{\rm max}^{(0)} = P_{\rm odd}^{(0)}(\alpha_{\rm max}) \approx 7.7866. \tag{23}$$

We stress that this prediction of the mobility threshold, i.e., the largest total power of the odd discrete soliton which may be set into motion by the arbitrarily large kick, is an unusual result even for the usual DNLS model with the purely cubic nonlinearity.

Finally, the weak quintic term, if treated as a small perturbation (see above), shifts the largest value of the total power, which admits the progressive motion, as

$$P_{\rm max} \approx P_{\rm max}^{(0)} + \nu P_{\rm max}^{(1)}, \tag{24}$$

with the coefficient found from the respective expansion of Eq. (20):

$$P_{\rm max}^{(1)} \approx \frac{2\sinh^4(\alpha_{\rm max})\tanh(\alpha_{\rm max})}{\sinh(2\alpha_{\rm max})+\sinh(4\alpha_{\rm max})}\left(P_{\rm max}^{(0)}\right)^2 \tag{25}$$

[recall $\alpha_{\rm max}$ is given by Eq. (22)]. At the same order $\sim\nu$, it is also necessary to include the correction to the VA-predicted total power, as given by Eq. (16). Thus, taking into regard both contributions, one from Eq. (25) and one from (17) with $\alpha=\alpha_{\rm max}$, our estimate for the largest total power admitting the mobility of the discrete soliton in Eq. (1), including the quintic term, is

$$\begin{aligned} P_{\rm max} &= P_{\rm max}^{(0)} - \nu\left[P_{\rm odd}^{(1)}(\alpha_{\rm max}) + P_{\rm max}^{(1)}\right] \\ &\approx 7.7866 - 72.0148\nu. \end{aligned} \tag{26}$$

Eventually, the absence of the mobility, alias "full stop" ($P_{\rm max}=0$), is predicted to occur at the following positive value of the quintic coefficient:

$$\nu_{\rm halt} = 0.1081. \tag{27}$$

On the other hand, Eq. (26) predicts that a negative quintic coefficient will produce the opposite effect, allowing mobility at larger values of power.

Comparing these predictions with numerical findings (see below), it is necessary to take into account that sufficiently heavy kicked localized modes first shed off a part of their power in the form of the lattice radiation waves ("phonons"). For this reason, the effective power which is predicted by Eqs. (23)–(26) is expected to be smaller than the actual initial power of the kicked modes. It is shown below that this expectation is borne out by the comparison with numerical results.

IV. NUMERICAL RESULTS FOR THE MODEL WITH SELF-FOCUSING CUBIC AND QUINTIC TERMS: $\gamma,\nu>0$

A. Stationary solutions

We start the numerical analysis by considering positive values of both nonlinear coefficients in Eq. (1): $\gamma,\nu>0$, which corresponds to both on-site nonlinear terms being *self-focusing*, in the optical context. First, we construct families of odd and even fundamental localized modes by solving Eq. (2), for propagation constants above the linear band. In Figs. 1 and 2 we show different families of odd and even fundamental solutions; insets show typical profiles of the odd and even fundamental modes. In general, with the increase of the quintic coefficient ν at constant propagation constant λ, we observe that the total power of the localized solutions decreases. Therefore, under the stronger self-focusing nonlinearity, it may be possible to excite strongly localized states at lower levels of power.

As we mentioned above, the stability of these solutions was predicted by means of a standard linear analysis; additionally, it was corroborated by direct simulations of their evolution in the framework of Eq. (1), adding initial white-noise perturbations. The odd mode is found to be unstable only in extremely

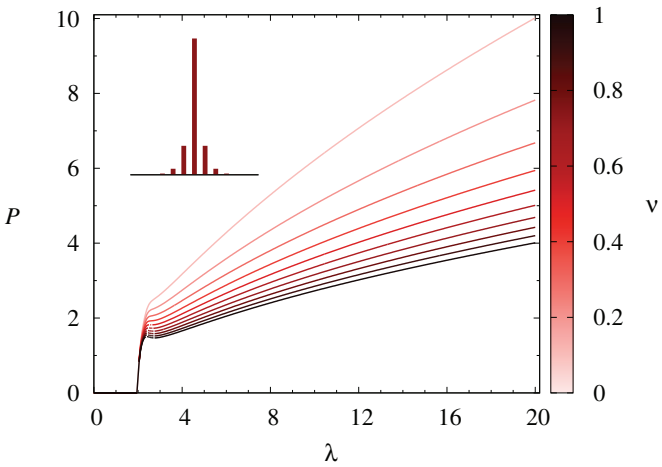

FIG. 1. (Color online) Total power P versus propagation constant λ for odd-mode (on-site-centered) soliton families. Each color corresponds to a different value of quintic coefficient ν, while the cubic coefficient is fixed to $\gamma=1$. The inset shows a typical profile of the odd localized mode for $P=2.4$, $\lambda=5.0$, and $\nu=0.5$.

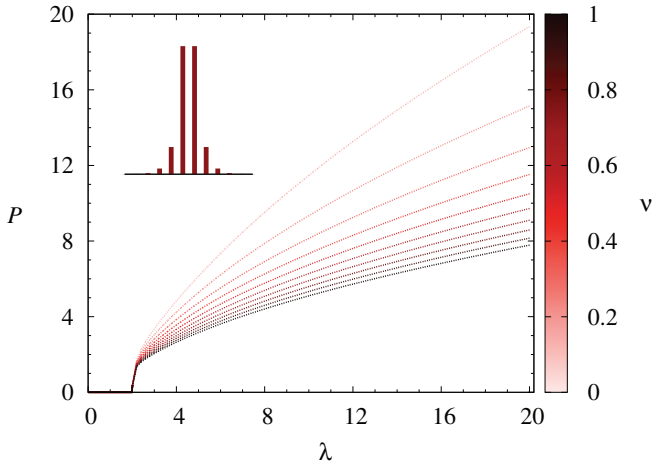

FIG. 2. (Color online) The same as in Fig. 1, but for the families of even (intersite-centered) modes. The inset shows a typical profile of the even localized mode for $P = 4$, $\lambda = 5.0$, and $\nu = 0.5$.

small portions of the $P(\lambda)$ curves with the negative slope $\partial P/\partial\lambda < 0$, in agreement with the Vakhitov-Kolokolov (VK) stability criterion [49]. On the other hand, the even mode is unstable in the whole range of explored parameters, which is a typical situation for cubic DNLS models [6]. In the course of the perturbed evolution, the stable odd modes radiate a very small amount of their power content and relax into the unperturbed shape. The unstable even modes radiate a significant amount of power and oscillate between the odd and even profiles.

To study the mobility of the localized modes, we first compute the PN barrier, which was defined above as the difference between the values of the Hamiltonian for the odd and the even modes [38]: $\Delta H \equiv H_{\rm odd} - H_{\rm even}$. Figure 3 displays a color map showing that the PN barrier monotonically increases with the total power and the positive quintic coefficient, ν. Therefore, in this parameter regime, the transport across the lattice is not expected to be enhanced.

It is relevant to point out here good agreement between the VA prediction and the numerical calculations. Indeed, it

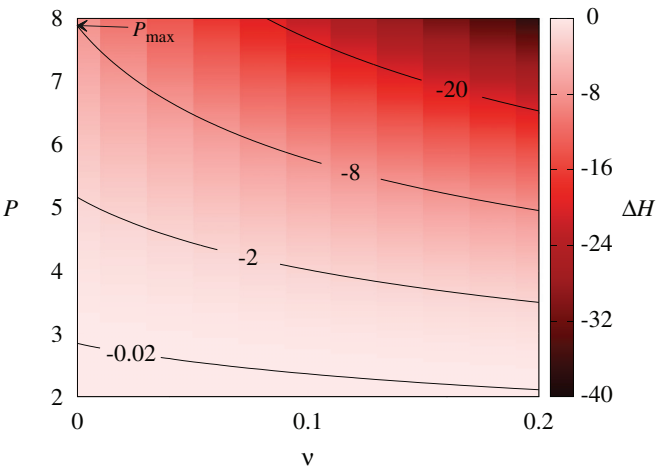

FIG. 3. (Color online) The color map of the PN barrier, ΔH, versus P and ν. The black arrow points out the VA of the $P_{\rm max}$ value.

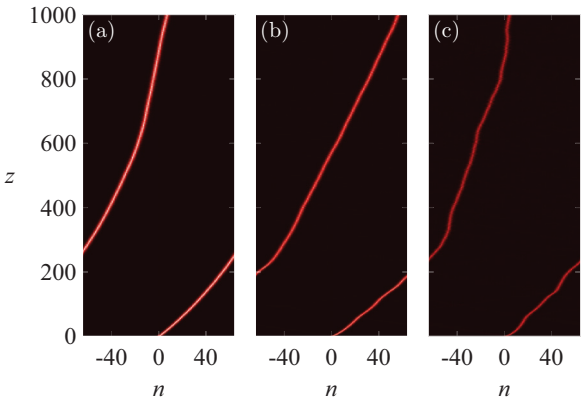

FIG. 4. (Color online) Examples of the mobility of discrete solitons across the whole lattice with $\gamma = 1$ and $\nu = 0$ (no quintic nonlinearity): (a) $P = 2.4$ and $k = 0.2$, (b) $P = 2.8$ and $k = 0.5$, and (c) $P = 3.2$ and $k = 0.8$.

follows from Eqs. (19), (22), and (23) that the largest kinetic energy which may be lent to the odd mode, at $\nu = 0$, is

$$E_{\rm kin} \approx 7.9954. \tag{28}$$

According to the prediction of the VA, this extra energy allows one to equalize the Hamiltonians of the odd and even modes; i.e., it must be equal to the PN barrier at the VA-predicted value of the total power, given by Eq. (23). The black arrow in Fig. 3 indicates this point, $P = P^0_{\rm max}, \nu = 0$, which belongs to the contour level of $\Delta H = -8$. The latter value is remarkably close to the VA prediction given by Eq. (28).

B. Dynamics

First, we consider the propagation of localized solutions in the system with the cubic-only nonlinearity, i.e., $\gamma = 1$ and $\nu = 0$ in Eq. (1). Figure 4 displays examples of clear mobility for three different powers and three different kicks: (a) $P = 2.4$ and $k = 0.2$, (b) $P = 2.8$ and $k = 0.5$ and (c) $P = 3.2$ and $k = 0.8$, in lattice with periodic boundary conditions. It is worthy to note that the trajectories gradually lose their smoothness as the power increases. Obviously, with the increase of the PN barrier the mobility deteriorates, in particular, due to the increment in the emission of radiation. Independent of the size of the kick, stationary modes with

$$P > \left(P^{(0)}_{\rm max}\right)_{\rm num} \approx 6 \tag{29}$$

stay immobile, losing a conspicuous part of their power in the form of radiation as a result of the application of the kick.

The comparison of the numerically found mobility threshold (29) with the VA-predicted counterpart (23) demonstrates a sufficiently reasonable agreement, taking into account that the VA for the moving discrete solitons cannot be developed in a highly accurate form, cf. Ref. [48]. The fact that the predicted threshold value of the power is greater than the numerically identified one is explained by the decrease of the power due to the radiative loss, as discussed above.

Now we include the effect of the quintic self-focusing nonlinearity, $\nu > 0$. As an example, we here take the same values $P = 3.2$ and $k = 0.8$ as in Fig. 4(c). As shown above in Fig. 3 and predicted by Eq. (26), the PN barrier increases

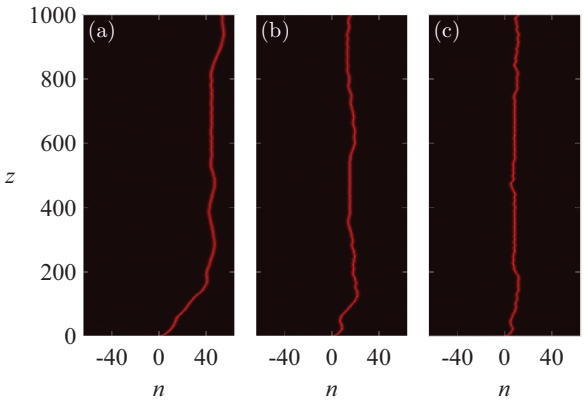

FIG. 5. (Color online) The mobility of discrete solitons with $P = 3.2$ under small values of the quintic coefficient: (a) $\nu = 0.01$, (b) $\nu = 0.03$, and (c) $\nu = 0.05$.

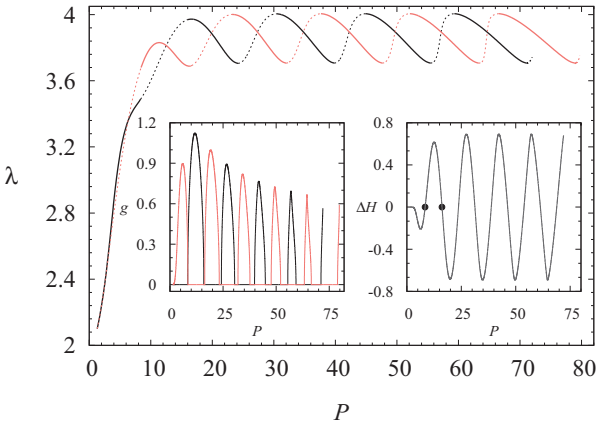

FIG. 6. (Color online) The propagation constant, λ, versus the total power, P, for families of odd (black) and even (red) discrete solitons in the system with $\gamma = 1$ and $\nu = -0.1$. Recall that continuous and dashed curves designate stable and unstable soliton families, respectively. The left inset shows the instability growth rate, g, for these families. The right inset shows the PN barrier corresponding to these solutions, in the whole domain.

monotonically with ν; hence, reduction of the mobility is expected. Figure 5 corroborates the dramatic reduction of the mobility while weakly increasing ν. At $\nu = 0.01$, the localized mode passes about 40 sites of the lattice [Fig. 5(a)], before getting trapped around $n = 41$. Increasing the quintic coefficient to $\nu = 0.03$ and then to $\nu = 0.05$, we observe that the discrete soliton shows erratic motion (it is explained by overcoming the potential barriers, losing the energy through the radiation loss, and facing new effectively lower barriers), before getting trapped around $n = 15$ [Fig. 5(b)] and $n = 10$ [Fig. 5(c)], respectively. Thus, the prediction of the VA that the quintic self-focusing term must completely suppress the mobility at rather small values of ν [see Eq. (27)] is in qualitative agreement with the numerical findings.

V. NUMERICAL RESULTS FOR THE MODEL WITH SELF-FOCUSING CUBIC AND DEFOCUSING QUINTIC TERMS: $\gamma > 0, \nu < 0$

A. Stationary solutions

The negative quintic coefficient, $\nu < 0$, implies saturation of the on-site self-focusing nonlinearity (as featured, e.g., by the photorefractive nonlinearity [8]). First, we look for fundamental stationary localized modes in this case. The respective solution families are constructed by fixing the total power and numerically looking for the corresponding mode profiles ϕ_n and the propagation constant λ; see Eq. (4). The results are displayed in Fig. 6 for $\gamma = 1$ and $\nu = -0.1$. We observe that, with the increase of the total power, the $\lambda(P)$ curves oscillate (sneak), odd (black) and even (red) modes, while the modal profiles increase their width by adding new sites in each oscillation, as shown in Fig. 7.

Below the first crossing point ($\lambda \approx 3.4$), the VK stability criterion applies. Then, the oscillations give rise to multiple stability exchanges at several crossing points. By increasing the total power, we observe regions where both, odd and even, solutions are unstable simultaneously, regions where only one solution is stable, and also regions where both solutions are *simultaneously stable*. The stability switching occurs, as it is generic for nonlinear dynamical systems [50–52], at saddle-node bifurcation points. In this case, these points coincide with maxima and minima values $\lambda(P)$ for $P > 15$. A variational approximation in the 'snaking' region was developed in Ref. [53]. This scenario is similar to the one known from the saturable nonlinearities and it is characterized by a continuous spatial broadening of the fundamental solutions, as a consequence of the saturation of the amplitude at large values of P; see Fig. 7.

On the other hand, by plotting the PN barrier, ΔH (right inset in Fig. 6), we observe several points at which it exactly vanishes, indicating that both solutions share their properties in the Hamiltonian representation; i.e., both are maxima or minima (unstable and stable states, respectively). A straightforward assumption was that at these points the system becomes "transparent" [54], featuring perfect mobility. However, a key ingredient was missing: When (at least) two solutions share stability properties, an extra solution in between must appear with the opposite stability. These intermediate stationary solutions typically correspond to asymmetric profiles. In the

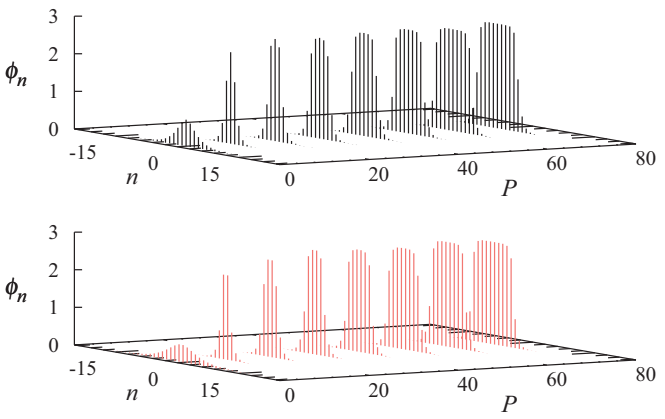

FIG. 7. (Color online) Solution profiles for the odd and even modes at several values of the total power (top and bottom panels, respectively) corresponding to the families represented by the black and red lines in Fig. 6.

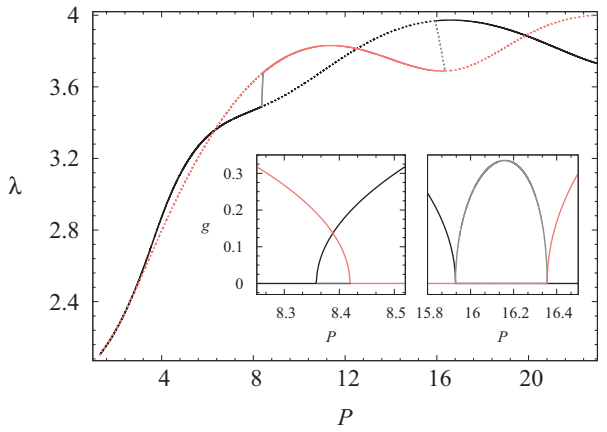

FIG. 8. (Color online) A zoom of the first stability-exchange region from Fig. 6. Asymmetric stable solutions family (the gray curves) appears as the connection between the odd- and even-mode families (black and red curves). The inset shows the instability growth rate, g, associated with the solutions belonging to the three different families.

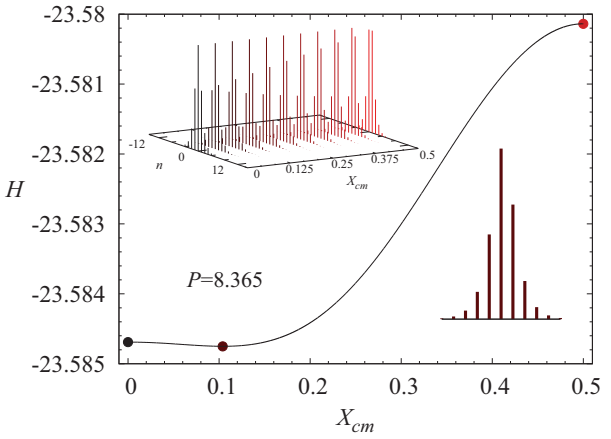

FIG. 9. (Color online) The H versus $X_{\rm cm}$ plot corresponding to the adiabatic transition between the odd- and even-mode solutions. The insets display asymmetric profiles of the intermediate solutions; see the text.

present case, for the competing CQ on-site nonlinearity, they were first found in Ref. [34]. With this ingredient included, the effective energy barrier is the one that takes into regard *all* stationary solutions in a certain region of the parameter space, rather than just the usual odd and even modes. This situation can be understood from the segment of $\lambda(P)$ curve in Fig. 6 which is magnified in Fig. 8. In this case, families of asymmetric solutions (gray branches) emerge, linking the odd and even families exactly at the stability-exchange points. They are associated with the two first vanishing points of the PN barrier, designated by the black solid circles in Fig. 6. Within a small total-power interval around $P \approx 8.4$, the odd and even families are simultaneously unstable. On the contrary, around $P = 16.1$ both of them are simultaneously stable. As the power increases, the PN barrier vanishes at several points, in accordance with oscillation of the $\lambda(P)$ curves and the exchange of the stability properties.

There are, essentially, two ways of obtaining the intermediate asymmetric solutions. The first one amounts to finding this solution dynamically, by tracing the center of mass of the wave packet and noticing when the velocity is smaller or larger, corresponding to a maxima or minima of the effective potential and, accordingly, to unstable or stable solutions [25,42]. The second, and more elegant, procedure is provided by the so-called "*constraint method*" [55,56]. It starts from a given stationary mode with defined propagation constant λ, power P, and center-of-mass coordinate X. We then implement a constrained Newton-Raphson method that finds solutions by keeping the power constant and varying X. By performing a smooth sweep in X, we are able to transform the profile from a given fundamental mode to the other one (e.g., from an odd mode to an even one). In Fig. 9 we show the $H(X)$ dependence obtained by implementing this method, including mode profiles of the constrained solutions. In fact, this process corresponds to a correct definition of the PN potential, the one which traces the shape of the effective potential that the mode must overcome while it moves adiabatically (without emission of radiation and keeping the power constant) from one site to another. As the system is periodic, this potential must be copied to construct the whole effective lattice potential. If there exists any intermediate stationary solution, it will correspond to a critical point on this diagram, depending on the particular model. The solid circles in Fig. 9 correspond to the stationary fundamental solutions for this level of power. The black and light red ones, located at $X = 0$ and $X = 0.5$, correspond to the unstable odd and even mode solutions. The extra critical point, the dark red solid circle located in between the other two ones, corresponds to a stable intermediate solution (potential minimum), with a characteristic profile sketched in the inset of Fig. 9.

When finding such an asymmetric mode, we construct the whole family by using a normal Newton-Raphson method. In Fig. 8 this family is shown by a gray line, connecting the fundamental odd and even modes in the region of multi-instability. As this solution corresponds to a minimum of the Hamiltonian (the ground state for this level total power), it is a stable solution located between two unstable ones [57].

We have computed the effective potential for the first *biunstable* region, by sweeping the value of the total power, P, and finding the Hamiltonian for all the constrained solutions in between the odd ($X = 0$) and even ($X = 0.5$) modes. To compare different effective potentials, we normalized the Hamiltonian to its maximum value for any level of the total power. Figure 10(a) displays a surface plot of the normalized values of H as a function of P and X. The center of mass of the stable asymmetric solutions passes from the odd mode to the even one, following the increase of P. For low levels of the total power the odd mode is stable and the even one unstable. Then, both solutions become unstable up to a level of the total power at which the even mode transforms into the ground state, and the odd mode transforms into an unstable solution. In that sense, the asymmetric intermediate solution plays the role of a *stability carrier*, which transfers the stability between the fundamental stationary solutions.

Next, we construct a similar energy landscape in a region where both fundamental solutions are simultaneously stable, around $P \approx 16.2$. This implies the existence of an intermediate

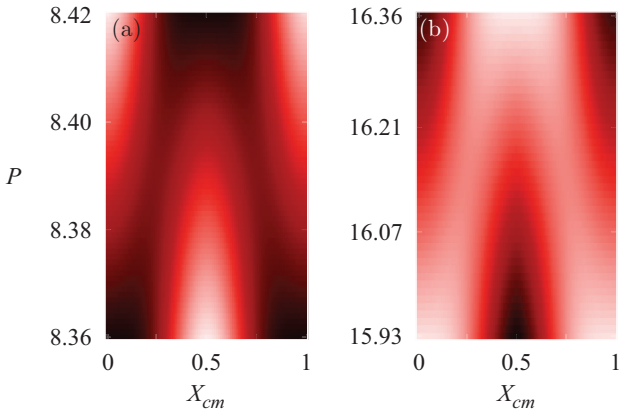

FIG. 10. (Color online) The color-map plot of the normalized Hamiltonian (H) for the intermediate solutions in the vicinity of stability-exchange points. (a) *Biunstable* region and (b) *bistable* region.

asymmetric unstable solution corresponding to a maximum between two minima (odd and even modes). The surface plot of the effective potential for this stability region, produced by the constraint method, is displayed in Fig. 10(b), which demonstrates that the intermediate solution is indeed unstable, and, in this region, it transfers the instability from one fundamental mode to the other, completely switching their stability properties.

B. Moving solitons

Having established the maps of the effective potential, we here address the mobility of the localized modes for powers above and below the threshold value $P_{\rm th}$, at which $\Delta H(P_{\rm th}) = 0$. We start by analyzing the evolution of unstable odd modes in the biunstable region, for a power below $P_{\rm th} \approx 8.39$ (see Fig. 10, where the value of H for the odd mode increases up to coinciding with that for the even mode). Below this power level, the odd modes do not have enough energy to overcome the PN barrier. Thus, the unstable odd modes oscillate in the interval of $-0.5 < X < +0.5$ without being able to cross the barrier. Figure 11 displays the evolution of X for several

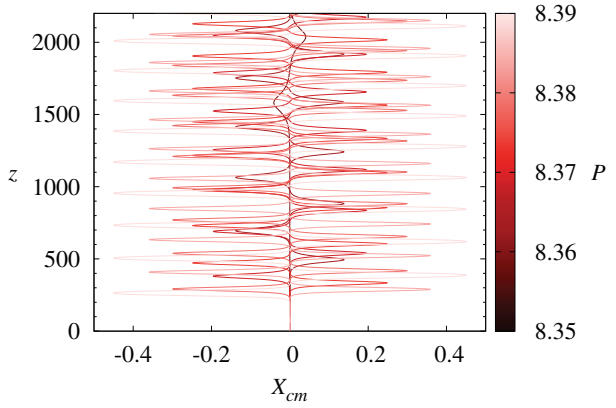

FIG. 11. (Color online) Oscillations of the center of mass ($X_{\rm cm}$) of unstable odd-mode solutions in the case of $P < P_{\rm th}$. Increase of the total power leads to larger oscillations amplitudes.

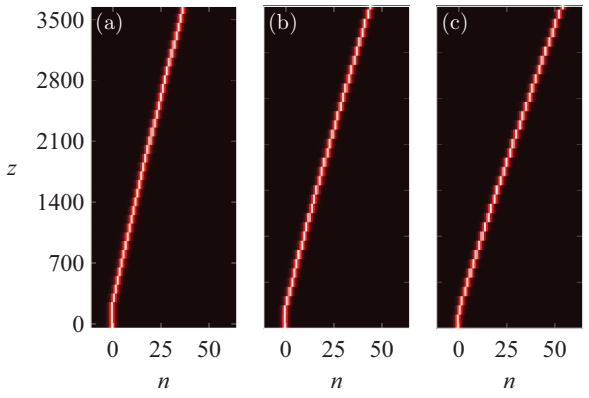

FIG. 12. (Color online) Dynamics of unstable odd-mode solutions for $P > P_{\rm th}$. (a) $P = 8.92$, (b) $P = 8.404$, and (c) $P = 8.414$.

unstable odd modes, all with $P < P_{\rm th}$. As the instability growth rate g increases, following the increase of the total power, the amplitude of the spontaneous oscillations increases too, because the value of H for the odd mode approaches that for the even one.

On the other hand, we observe mobility of the localized modes at $P > P_{\rm th}$, where the value of H for the odd mode is larger than the even one. Therefore, the odd mode is able to overcome the PN barrier and move across the lattice. Figure 12 shows the evolution of three different unstable odd-mode solutions for three different levels of the total power. We observe that the transversal velocity of the spontaneous motion is correlated to the power; for example, in case (c) the velocity almost doubles in comparison with case (a). For an increasing power, the value of H for the odd mode increases in comparison to the even mode. Therefore, the kinetic energy for this mode is larger, letting it move faster across the lattice.

We proceed to exploring the next stability-exchange region, located around $P \approx 16.14$. Here, both fundamental solutions are stable and both correspond to minima of the Hamiltonian, without starting spontaneous motion. Therefore, a kick must be applied to these modes to help them overcome the energy barriers. The kick with $k = 0.1$ was enough to set into motion all the odd stable modes in this region. Figure 13 displays the motion of the center of mass, X, for several kicked odd modes with different total powers. After passing a certain distance, some the kicked discrete solitons come to a halt (see the top inset), getting trapped between two sites of the lattice, while others continue the persistent motion. We observe that the final values of X, at which the motion ceases, increases with the total power of the soliton in this region of parameters. On the other hand, Fig. 13 also shows that the discrete solitons with smaller total powers initially move faster than ones with greater powers. This feature can be easily explained by the comparison with the NLS equation in continuum, where the kick measures the momentum imparted to the soliton, while the total power determines its mass; hence, the heavier soliton moves slower under the action of the same kick.

The difference in the mobility between the lighter and the heavier solitons, kicked with the same strength, is shown in more detail in Fig. 14, where the soliton field is displayed on the logarithmic scale: The shape distortion, manifested by the generation of radiation tails, is greater for lighter solitons

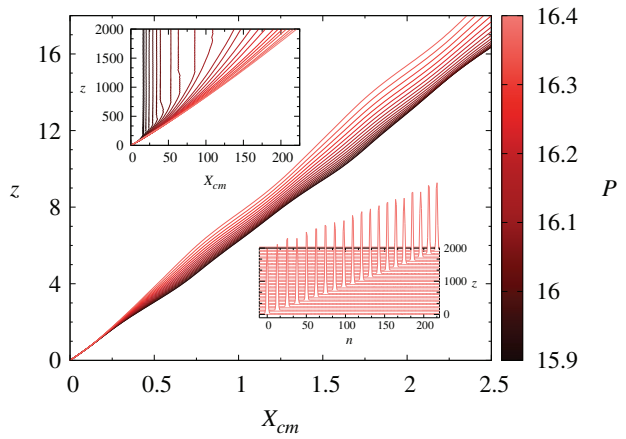

FIG. 13. (Color online) The initial stage of the motion of the center of mass, $X_{\rm cm}$, of stable odd-mode solutions, with $15.93 < P < 16.36$, under the action of kick $k = 0.1$. The top inset shows long-scale evolution of these modes. The bottom inset illustrates the robust mobility of the mode with $P = 16.36$.

[Fig. 14(a)]. Thus, the heavier ones are more stable in the traveling state [Fig. 14(b)], as shown by the bottom inset in Fig. 13, which displays the persistent motion of the discrete soliton with total power $P = 16.4$. Therefore, the heavier solitons are more appropriate for applications related to transport properties.

VI. COLLISIONS BETWEEN MOVING SOLITONS

Once the regions with mobility of the discrete solitons having been established, it is natural to consider collisions between two traveling robust solitons, which are set in motion by kicks in opposite direction. The corresponding input can be written as

$$\psi_n(z=0) = \phi_n^{(1)} e^{ik_1(n-n1)} + \phi_n^{(2)} e^{ik_2(n-n2)}, \qquad (30)$$

where n_1 and n_2 are the initial positions of centers of the stationary solutions, $\phi^{(1)}$ and $\phi^{(2)}$, respectively.

Figure 15 displays different scenarios of the interaction between identical colliding modes. The first case [Fig. 15(a)] shows the interaction between two discrete solitons initially

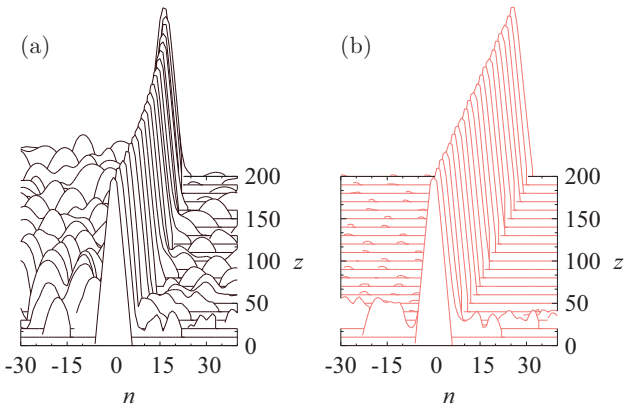

FIG. 14. (Color online) Amplitude profiles, on the logarithmic scale, of two moving solitons, both kicked by $k = 0.1$. Left, $P = 15.93$; right, $P = 16.36$.

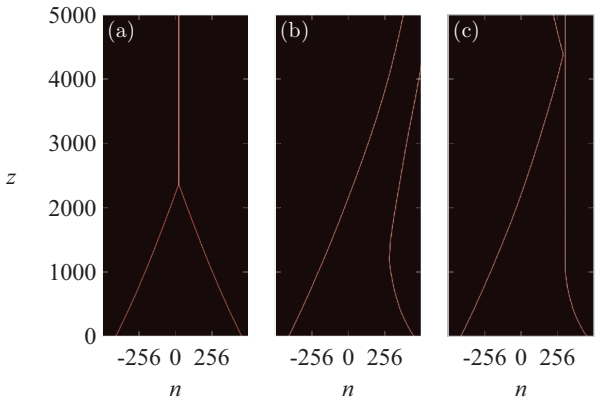

FIG. 15. (Color online) Three different scenarios of collisions between traveling discrete solitons: merger for $k_1 = -k_2 = 0.1$ (a), rebound for $k_1 = 0.1$ and $k_2 = -1.9$ (b), and the formation of the signal-blocker pair for $k_1 = 0.1$ and $k_2 = -0.2$ (c).

kicked with $k_1 = -k_2 = 0.1$. After the collision, they merge into a single quiescent structure with the double total power. In another case [Fig. 15(b)], the collision does not take place, due to repulsion between the solitons (*rebound*). The stronger kicked mode, with $k_2 = -1.9$, changes the direction of its velocity, and keeps moving almost at the same velocity as the other mode, which was kicked by $k_1 = 0.1$. Finally, when the two modes are kicked by $k_1 = 0.1$ and $k_2 = -0.2$, the interaction between them resembles that of a *signal-blocker pair*; i.e., one discrete soliton gets trapped, producing a barrier for the perfect reflection of the other soliton [see Fig. 15(c)].

The interaction picture observed in panels (b) and (c) of Fig. 15 suggests that the interaction between the discrete solitons may feature effectively long-range interactions. This may be explained by the interaction of the phonon (radiation) tail of each soliton, such as those observed in Fig. 14, with the body of the other; cf. a similar mechanism considered earlier in continuous media [58].

VII. CONCLUSION

In this work, we used the 1D DNLS model with the CQ on-site nonlinearity to investigate fundamental mobility regimes for discrete solitons. The cubic term was taken, as usual, with the self-focusing sign, while both signs of the quintic term were considered separately, as well as the usual cubic model, when the quintic term is absent. The analytical part of the work was based on the VA, with the aim to estimate the mobility threshold, i.e., the largest value of the discrete-soliton's total power (norm) which admits free motion of the kicked soliton. This was done by comparing the largest possible value of the soliton's effective kinetic energy with the height of the PN potential barrier. It is relevant to stress that this analytical prediction is unusual also for the usual DNLS equation with the purely cubic nonlinearity. The prediction was found to be in a reasonable agreement with numerical results. In addition, this analytical estimate qualitatively predicts that the increase of the coefficient in front of self-focusing quintic term quickly suppresses the mobility. In the DNLS model with competing self-focusing and defocusing CQ terms, we have identified, by means of the numerical analysis, regions in

the parameter space where even and odd fundamental modes exchange their stability, which involves the appearance of intermediate asymmetric modes. In this case, stable solitons are kicked to overcome the PN barrier and get in a state of persistent motion. On the other hand, it has been demonstrate by means of direct simulations that unstable solitons start progressive motion spontaneously, provided that they initially exist above the mobility threshold. Finally, collisions between stable moving discrete solitons were considered, and three different scenarios identified for them.

The analysis reported here may be extended in other directions. In particular, it may be interesting to consider possible mobility of excited (nonfundamental) localized states, such as twisted modes [59]. A challenging problem is to generalize the analysis for those 2D models where mobile modes may exist [25,26].

ACKNOWLEDGMENTS

C.M.-C. thanks Uta Naether and Mario I. Molina for valuable discussions. We acknowledge funding support from FONDECYT Grant No. 1110142, Programa ICM P10-030-F, and Programa de Financiamiento Basal de CONICYT (Grant No. FB0824/2008). B.A.M. appreciates hospitality of the Faculty of Engineering and Applied Sciences at the Universidad de los Andes (Santiago, Chile).

[1] A. Hasegawa, Opt. Photon. News **13**, 33 (2002).
[2] J. S. Aitchison, Y. Silberberg, A. M. Weiner, D. E. Leaird, M. K. Oliver, J. L. Jackel, E. M. Vogel, and P. W. E. Smith, J. Opt. Soc. Am. B **8**, 1290 (1991).
[3] J. W. Fleischer, M. Segev, N. K. Efremidis, and D. N. Christodoulides, Nature (London) **422**, 147 (2003).
[4] D. N. Christodoulides, F. Lederer, and Y. Silberberg, Nature (London) **424**, 817 (2003).
[5] S. Flach and C. R. Willis, Phys. Rep. **295**, 181 (1998).
[6] P. G. Kevrekidis, *The Discrete Nonlinear Schrödinger Equation: Mathematical Analysis, Numerical Computations and Physical Perspectives*, Springer Tracts in Modern Physics (Springer-Verlag Berlin Heidelberg, 2009).
[7] H. S. Eisenberg, R. Morandotti, Y. Silberberg, J. M. Arnold, G. Pennelli, and J. S. Aitchison, J. Opt. Soc. Am. B **19**, 2938 (2002).
[8] N. K. Efremidis, S. Sears, D. N. Christodoulides, J. W. Fleischer, and M. Segev, Phys. Rev. E **66**, 046602 (2002).
[9] A. A. Sukhorukov, Y. S. Kivshar, H. S. Eisenberg, and Y. Silberberg, IEEE J. Quantum Electron. **39**, 31 (2003).
[10] F. S. Cataliotti, L. Fallani, F. Ferlaino, C. Fort, P. Maddaloni, and M. Inguscio, New J. Phys. **5**, 71 (2003).
[11] F. K. Abdullaev, B. B. Baizakov, S. A. Darmanyan, V. V. Konotop, and M. Salerno, Phys. Rev. A **64**, 043606 (2001).
[12] G. L. Alfimov, P. G. Kevrekidis, V. V. Konotop, and M. Salerno, Phys. Rev. E **66**, 046608 (2002).
[13] G. Gligorić, A. Maluckov, L. Hadžievski, and B. A. Malomed, Phys. Rev. A **78**, 063615 (2008).
[14] G. Gligorić, A. Maluckov, M. Stepic, L. Hadžievski, and B. A. Malomed, Phys. Rev. A **81**, 013633 (2010).
[15] A. V. Ustinov, M. Cirillo, and B. A. Malomed, Phys. Rev. B **47**, 8357 (1993).
[16] M. V. Fistul, Chaos **13**, 725 (2003).
[17] J. J. Mazo and T. P. Orlando, Chaos **13**, 733 (2003).
[18] T. Dauxois, M. Peyrard, and A. R. Bishop, Phys. Rev. E **47**, R44 (1993).
[19] M. Peyrard, T. Dauxois, H. Hoyet, and C. Willis, Physica D **68**, 104 (1993).
[20] A. B. Aceves, C. D. Angelis, S. Trillo, and S. Wabnitz, Opt. Lett. **19**, 332 (1994).
[21] R. A. Vicencio, M. I. Molina, and Y. S. Kivshar, Opt. Lett. **28**, 1942 (2003).
[22] J. Cuevas, B. A. Malomed, and P. G. Kevrekidis, Phys. Rev. E **71**, 066614 (2005).
[23] R. Morandotti, U. Peschel, J. S. Aitchison, H. S. Eisenberg, and Y. Silberberg, Phys. Rev. Lett. **83**, 2726 (1999).
[24] U. Peschel, R. Morandotti, J. M. Arnold, J. S. Aitchison, H. S. Eisenberg, Y. Silberberg, T. Pertsch, and F. Lederer, J. Opt. Soc. Am. B **19**, 2637 (2002).
[25] R. A. Vicencio and M. Johansson, Phys. Rev. E **73**, 046602 (2006).
[26] H. Susanto, P. G. Kevrekidis, R. Carretero-Gonzalez, B. A. Malomed, and D. J. Frantzeskakis, Phys. Rev. Lett. **99**, 214103 (2007).
[27] U. Naether, R. A. Vicencio, and M. Stepić, Opt. Lett. **36**, 1467 (2011).
[28] O. A. Egorov and F. Lederer, Opt. Lett. **38**, 1010 (2013).
[29] A. Maluckov, L. Hadžievski, and B. A. Malomed, Phys. Rev. E **77**, 036604 (2008).
[30] D. K. Campbell, S. Flach, and Y. S. Kivshar, Phys. Today **57**(1), 43 (2004).
[31] F. Lederer, G. I. Stegeman, D. N. Christodoulides, G. Assanto, M. Segev, and Y. Silberberg, Phys. Rep. **463**, 1 (2008).
[32] S. Flach and A. V. Gorbach, Phys. Rep. **467**, 1 (2008).
[33] M. Elstner, D. Porezag, G. Jungnickel, J. Elsner, M. Haugk, T. Frauenheim, S. Suhai, and G. Seifert, Phys. Rev. B **58**, 7260 (1998).
[34] R. Carretero-Gonzlez, J. D. Talley, C. Chong, and B. A. Malomed, Physica D **216**, 77 (2006).
[35] C. Chong, R. Carretero-Gonzlez, B. A. Malomed, and P. G. Kevrekidis, Physica D **238**, 126 (2009).
[36] F. Lederer, S. Darmanyan, and A. Kobyakov, in *Nonlinearity and Disorder: Theory and Applications*, edited by F. Abdullaev, O. Bang, and M. Sörensen, NATO Science Series, Vol. 45 (Springer, Netherlands, 2001), pp. 131–157.
[37] A. Khare, K. Ø. Rasmussen, M. R. Samuelsen, and A. Saxena, J. Phys. A: Math. Gen. **38**, 807 (2005).
[38] Y. S. Kivshar and D. K. Campbell, Phys. Rev. E **48**, 3077 (1993).
[39] D. Guzmán-Silva, C. Lou, U. Naether, C. E. Rüter, D. Kip, and R. A. Vicencio, Phys. Rev. A **87**, 043837 (2013).
[40] U. Naether, R. A. Vicencio, and M. Johansson, Phys. Rev. E **83**, 036601 (2011).
[41] S. Rojas-Rojas, R. A. Vicencio, M. I. Molina, and F. K. Abdullaev, Phys. Rev. A **84**, 033621 (2011).
[42] R. A. Vicencio and M. Johansson, Phys. Rev. A **87**, 061803 (2013).
[43] C. Chong and D. Pelinovsky, Discrete and Continuous Dynamical Systems **4**, 1019 (2011).

[44] D. B. Duncan, J. C. Eilbeck, H. Feddersen, and J. A. D. Wattis, Physica D **68**, 1 (1993).
[45] S. Flach and K. Kladko, Physica D **127**, 61 (1999).
[46] S. Flach, Y. Zolotaryuk, and K. Kladko, Phys. Rev. E **59**, 6105 (1999).
[47] M. J. Ablowitz, Z. H. Musslimani, and G. Biondini, Phys. Rev. E **65**, 026602 (2002).
[48] I. E. Papacharalampous, P. G. Kevrekidis, B. A. Malomed, and D. J. Frantzeskakis, Phys. Rev. E **68**, 046604 (2003).
[49] N. G. Vakhitov and A. A. Kolokolov, Radiophys. Quantum Electron. (Engl. Transl.) **16**, 783 (1973).
[50] J. Burke and E. Knobloch, Chaos **17**, 037102 (2007).
[51] G. Herring, P. G. Kevrekidis, R. Carretero-Gonzlez, B. A. Malomed, D. J. Frantzeskakis, and A. R. Bishop, Phys. Lett. A **345**, 144 (2005).
[52] A. Sacchetti, Phys. Rev. Lett. **103**, 194101 (2009).
[53] P. C. Matthews and H. Susanto, Phys. Rev. E **84**, 066207 (2011).
[54] L. Hadžievski, A. Maluckov, M. Stepić, and D. Kip, Phys. Rev. Lett. **93**, 033901 (2004).
[55] M. I. Molina, R. A. Vicencio, and Y. S. Kivshar, Opt. Lett. **31**, 1693 (2006).
[56] C. R. Rosberg, D. N. Neshev, W. Królikowski, A. Mitchell, R. A. Vicencio, M. I. Molina, and Y. S. Kivshar, Phys. Rev. Lett. **97**, 083901 (2006).
[57] V. I. Arnol'd, *Mathematical Methods of Classical Mechanics*, Graduate Texts in Mathematics (Springer, Berlin, 1989).
[58] B. A. Malomed, Phys. Rev. E **47**, 2874 (1993).
[59] S. Darmanyan, A. Kobyakov, and F. Lederer, J. Exp. Teor. Phys. **86**, 682 (1998).